Supplementary Information for

Recurrent rewiring of the adult hippocampal mossy fiber system by a single transcriptional regulator, Id2

Wenshu Luo[1], Matteo Egger[1], Andor Domonkos[1], Lin Que[1], David Lukacsovich[1], Natalia Cruz-Ochoa[1], Szilárd Szőcs[2], Charlotte Seng[1], Antónia Arszovszki[3], Eszter Sipos[3], Irmgard Amrein[4], Jochen Winterer[1], Tamás Lukacsovich[1], János Szabadics[3], David Wolfer[4,5], Csaba Varga[2] and Csaba Földy[1,*]

[1] Laboratory of Neural Connectivity, Brain Research Institute, Faculties of Medicine and Science, University of Zürich, Switzerland
[2] Szentágothai Research Center, Department of Physiology, Medical School, University of Pécs, Hungary
[3] Laboratory of Cellular Neuropharmacology, Institute of Experimental Medicine, Budapest, Hungary
[4] Institute of Anatomy, Faculty of Medicine, University of Zürich, Switzerland
[5] Institute of Human Movement Sciences and Sport, D-HEST, ETH Zürich, Switzerland
* Correspondence: Csaba Földy (foldy@hifo.uzh.ch)

This file includes:

List of Supplementary Figures and Tables:

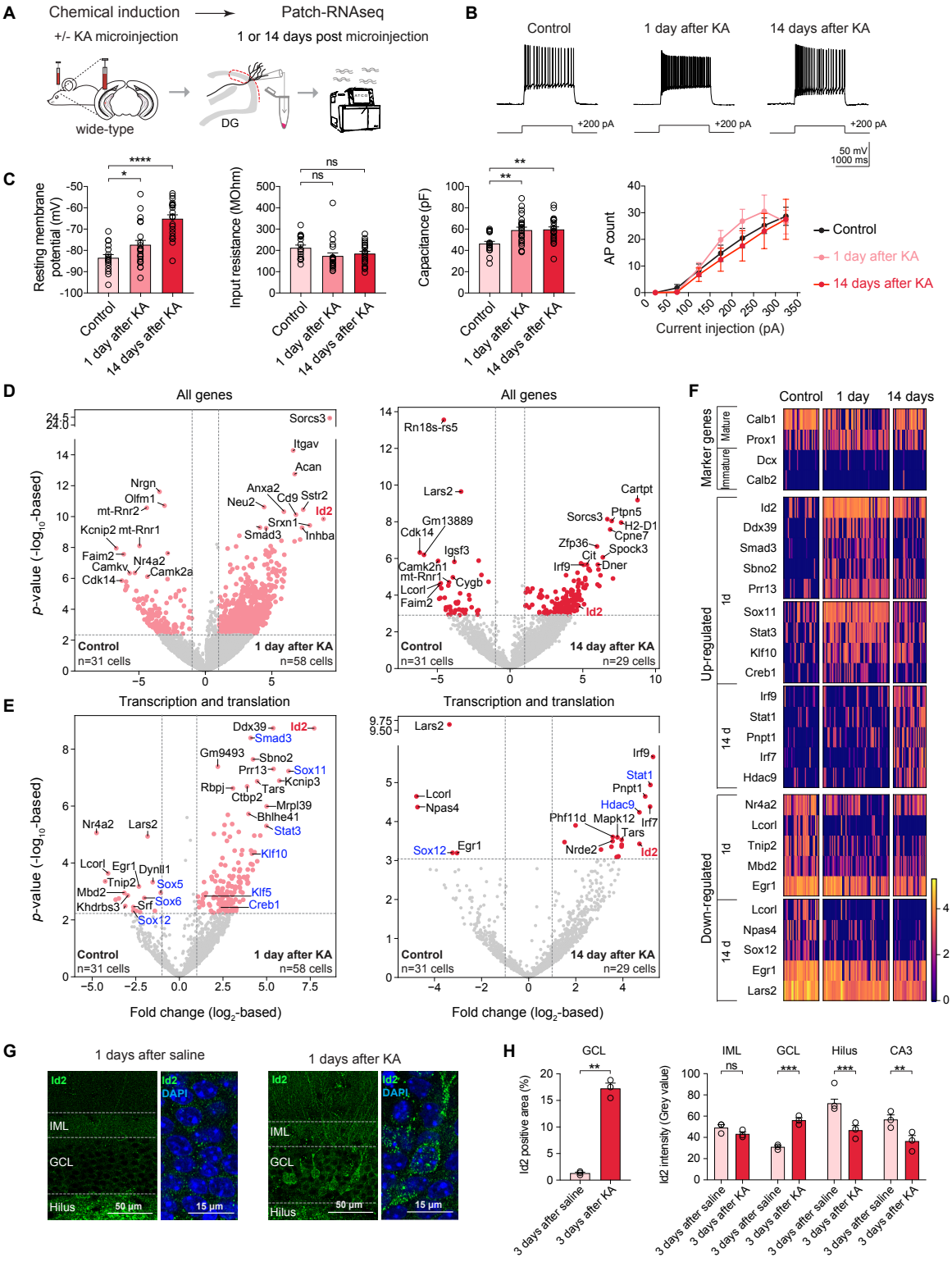

Fig. S1 | Analysis of KA-induced electrophysiological and transcriptomic changes

(A) In brain slices, patch-clamp recordings and single-cell RNAseq (Patch-RNAseq) were used to sample single dentate GCs for their electrophysiological properties and transcriptomic content 1 and 14 days after KA induction of MF sprouting.

(B) Example electrophysiological traces show GC response to 1.5 s long current pulse injections. GCs from age-matched, non-injected animals were used as control.

(C) Quantification of biophysical (data points represent single cells, Control, n=17 cells / 2 mice; 1 day after KA, n=23 cells / 3 mice; 14 days after KA, n=21 cells / 2 mice. Resting membrane potential, one-way ANOVA: F=23, p<0.0001, post-hoc: Control vs 1 day after KA, *p=0.030, Control vs 14 days after KA, ****p<0.0001; Input resistance, one-way ANOVA: F=2.0, p=0.14; Capacitance, one-way ANOVA: F=7.2, p=0.0016, post-hoc: Control vs 1 day after KA, **p=0.0016, Control vs 14 days after KA, **p=0.0012) and action potential firing properties (AP count; note that for comparability, only those cells were included in this analysis, whose initial resting membrane potential was between -70 and -85 mV; Control, n=11 cells, 1 day after KA, n=11 cells, 14 day after KA, n=7 cells, two-way ANOVA, F_{Phase} (6,154)=66, p<0.0001; $F_{Treatment}$ (2,26)=0.39, p=0.68; $F_{Treatment\ x\ Phase}$ (12,154) =1.0, p=0.45).

(D) Volcano plots show acute (compared to controls, 1 day after KA, left) and persistent (14 days after KA, right) transcriptomic changes in single GCs after KA induction of MF sprouting. Red points denote differentially expressed genes (FDR<0.05 and >2-fold change, $|\log_2 FC|>1$).

(E) Volcano plots show acute (1 day after KA, left; same as in main Fig. 1) and persistent (14 days after KA, right) transcriptomic changes of transcription and translation-related molecules in single GCs after KA induction of MF sprouting. Red points denote differentially expressed genes (FDR<0.05 and >2-fold change, $|\log_2 FC|>1$). Gene names highlighted with blue were previously associated with axon growth.

(F) Heat map shows the expression of mature and immature GC markers, as well as up- and down-regulated transcription and translation-related molecules (from panel E) in single GCs.

(G) Confocal images show Id2 and DAPI immunostaining 1 day after intrahippocampal saline (left panels) and KA injections (right panels.

(H) Quantification of Id2 immunostaining signal intensity in hippocampus 3 days after KA induction. Left: Id2 positive area in GCL (3 days after saline, 1.3±0.19, 3 mice; 3 days after KA, 17±0.98, 3 mice; Welch's t-test, **p=0.0028). Right: Id2 signal intensity (grey value) in IML, GCL, Hilus, and CA3 (two-way ANOVA, F_{Area} (3,12)=24, p<0.001; $F_{Treatment}$ (1,4)=2.3, p=0.20; $F_{Area\ x\ Treatment}$ (3,12)=61, p<0.0001; post-hoc analyses: 3 days after saline vs 3 days after KA, IML, p=0.25; GCL, ***p=0.0001; Hilus, ***p=0.0001; CA3, **p=0.0009).

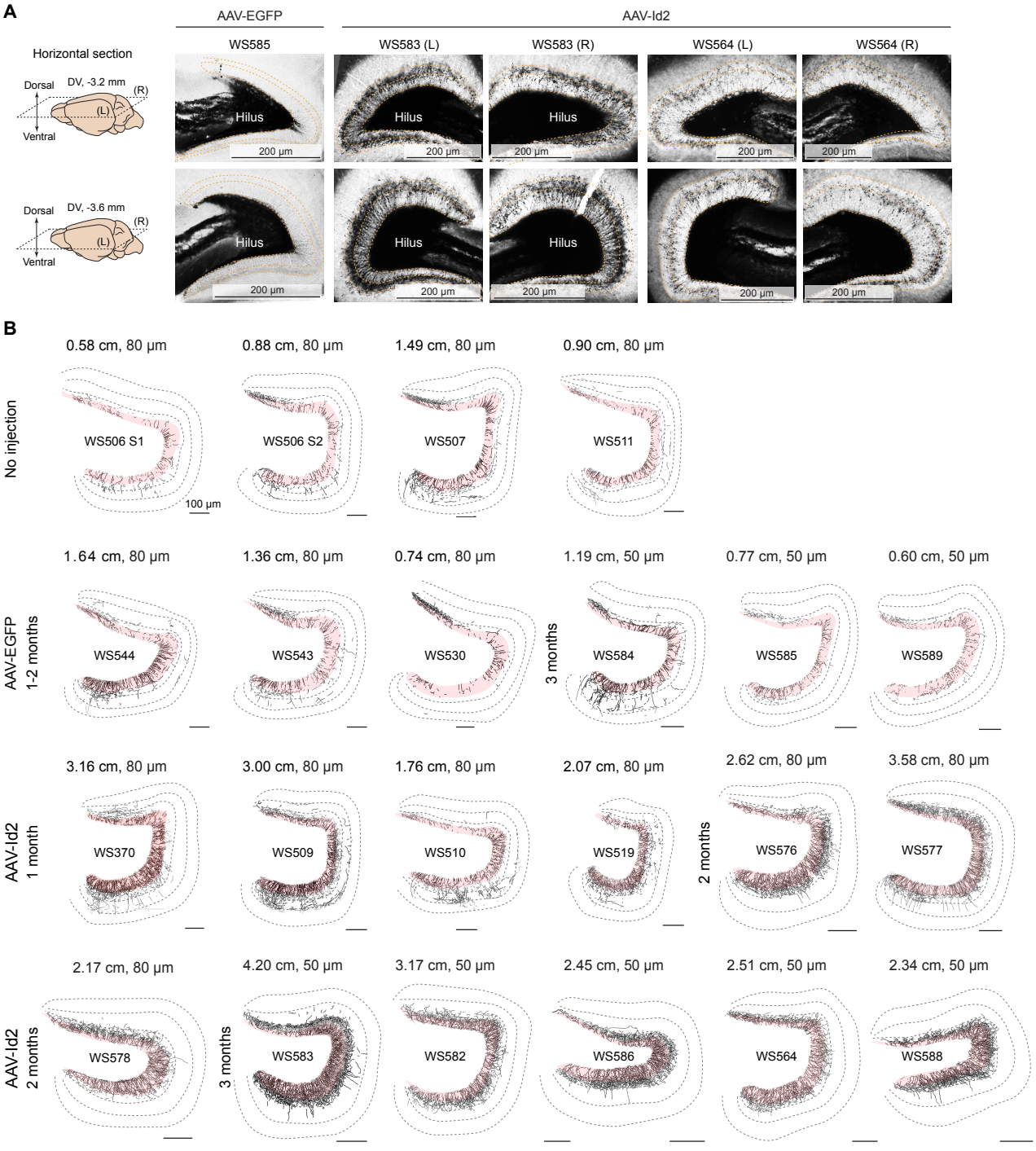

Fig. S2 | Reconstruction of MF axon growth induced by AAV-Id2

(A) Images show Timm's-stained sections collected from ventral hippocampus after AAV-EGFP (control) and AAV-Id2 injections. Sample IDs and hemispheres (left, L, or right, R) are indicated above the images.

(B) Timm's staining-based MF axon tracings in control circuits (no injection, and 1-2 and 3 months after AAV-EGFP injection) and 1, 2 and 3 months after AAV-Id2 injection. Brain sections were either 50 or 80 µm thick as indicated above each image. For each image, total measured axon length (in cm), section thickness (in µm) and sample ID are shown. Quantification of section thickness-normalized total axon length is shown in Fig. 2, where AAV-EGFP controls were pooled independent of sampling schedule (non-injected controls were not included).

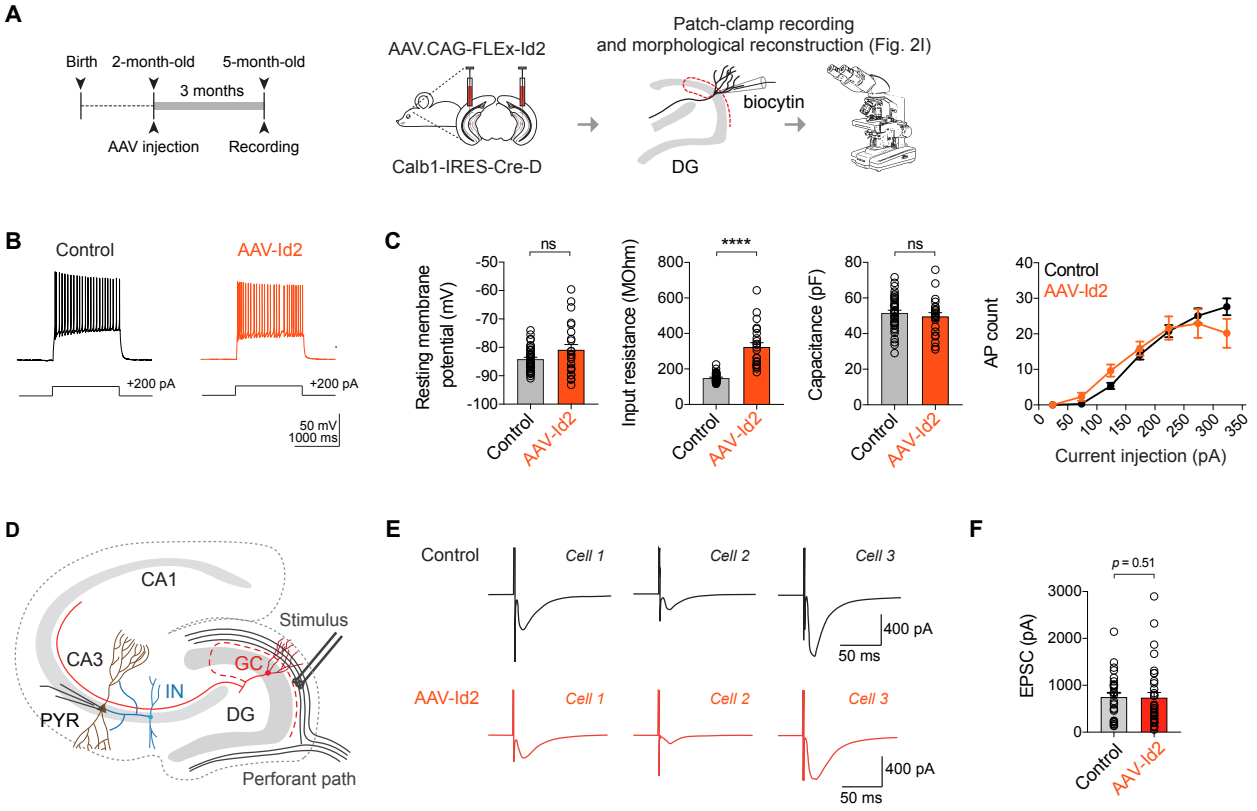

Fig. S3 | Biophysical properties of GCs and MF output in CA3 after AAV-Id2 delivery

(A) Experimental design.

(B) Example electrophysiological traces show GC response 1.5 s long current pulse injections. GCs from age-matched, non-injected animals were used as control.

(C) Quantification of biophysical (data points represent single cells, Control, n=40 cells / 2 mice, AAV-Id2, 3 months after injections, n=23 cells / 2 mice; using Mann-Whitney *U* test: Resting membrane potential, p=0.40; Input resistance, ****p<0.0001; Capacitance, p=0.37) and action potential firing properties (AP count; note that for comparability, only those cells were included in this analysis, whose initial resting membrane potential was between -80 and -90 mV (Control, n= 32 cells, AAV-Id2, n=12 cells, two-way ANOVA: F_{Phase} (6,248)=82, p<0.0001; $F_{Treatment}$ (1,42)=0.0026, p=0.96; $F_{Treatment\ x\ Phase}$ (6,248) =2.7, p=0.014; post-hoc analyses: Control vs AAV-Id2: 25, p>0.99, 75, p=0.47, 125, p=0.13, 175, p=0.52, 225, p=0.76, 275, p=0.44, 325, p=0.011, q=0.077, does not meet FDR criterion).

(D) To test the overall synaptic drive of the dentate gyrus onto CA3 (which involves direct MF and indirect feed-forward interneuron, IN, transmission onto CA3 pyramidal cells, PYR), we extracellularly stimulated the perforant path while intracellularly recorded from CA3 PYRs 3 months after AAV-EGFP (control) and AAV-Id2 injections. Stimulation intensity (5 mA), frequency (0.2 Hz) and duration (1 ms) were kept constant across recordings.

(E) Example evoked events.

(F) Averaged peak amplitudes in ACSF in presence of 10 µM Gabazine (EPSC; Control: 747±93 pA, n=28 cells / 4 mice; AAV-Id2: 737±110 pA, n=35 cells / 6 mice; circles represent single cells; Mann-Whitney *U* test).

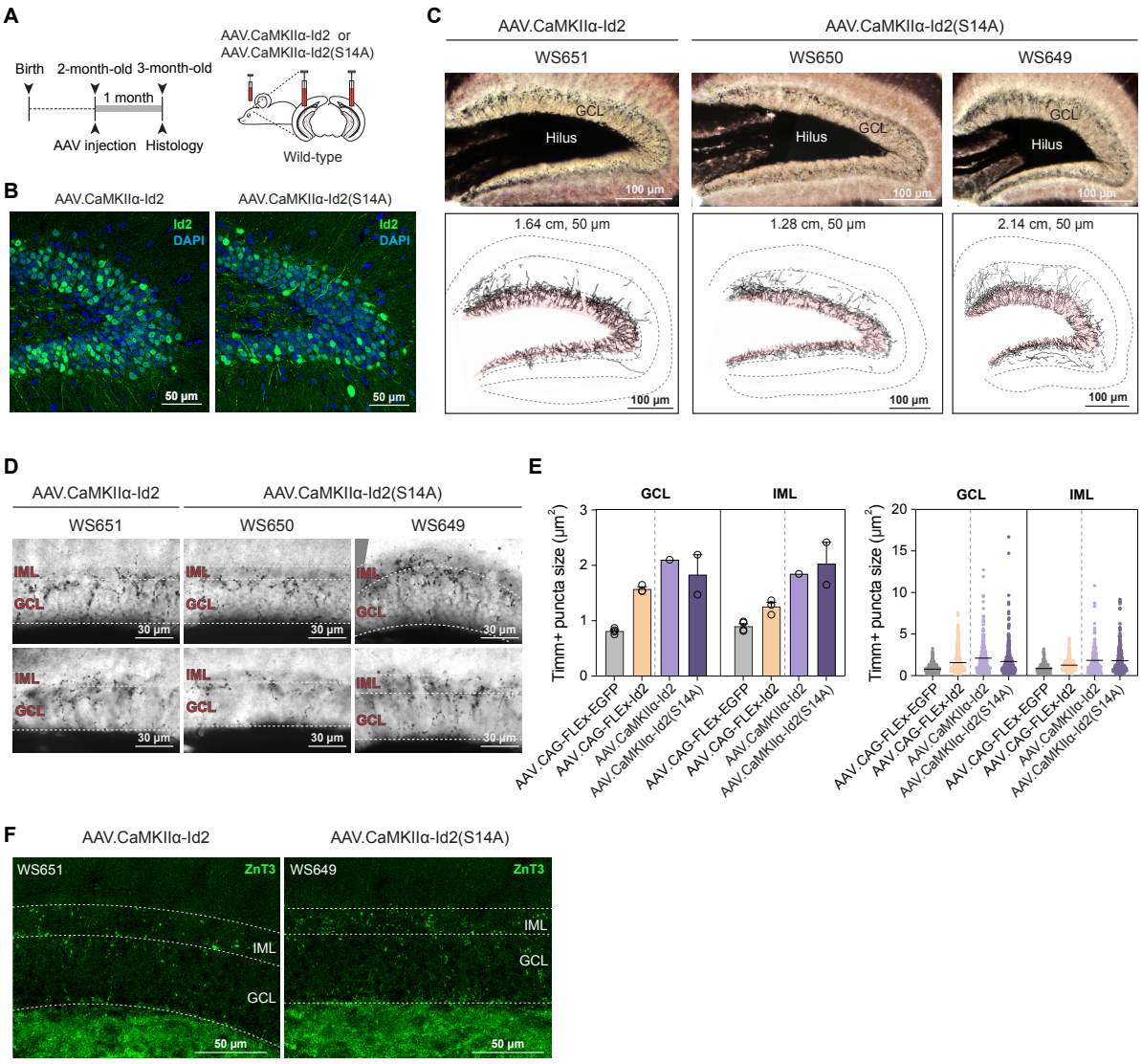

Fig. S4 | Id2 induced MF rewiring independently of its phosphorylation at S14

(A) Experimental design. Wild type (AAV.CaMKIIα-Id2) or S14 phosphorylation deficient Id2 (AAV.CaMKIIα-Id2(S14A)) viral constructs were injected into the ventral hippocampus. Brain sections were prepared and analyzed 1 month later.

(B) Confocal images show that Id2 immunostaining and subcellular localization was similar after AAV.CaMKIIα-Id2 and AAV.CaMKIIα-Id2(S14A) injections.

(C) Upper images show Timm's-stained sections collected from ventral hippocampus one month after AAV.CaMKIIα-Id2 and AAV.CaMKIIα-Id2(S14A) injections. Lower images show Timm's staining-based MF axon tracings form the same sections.

(D) Higher magnification images show MF rewiring in GCL/IML after both AAV.CaMKIIα-Id2 and AAV.CaMKIIα-Id2(S14A) injections.

(E) Quantification of Timm's positive puncta size in GCL/IML after Cre-dependent EGFP and 1 month after Cre-dependent Id2 overexpression in Calb-IRES-Cre mice (the same data as in Fig. 2*E* shown for comparison), and 1 month after AAV.CaMKIIα-Id2 and AAV.CaMKIIα-Id2(S14A) injections in wild-type mice. Left panel: data points represent puncta size averages per individual mouse. Right panel: data points represent individual puncta from all mice in each category, mean puncta size values are indicated with horizontal lines.

(F) ZnT3 imunostaining show MF synapses in GCL/IML 1 months after AAV.CaMKIIα-Id2 and AAV.CaMKIIα-Id2(S14A) injections.

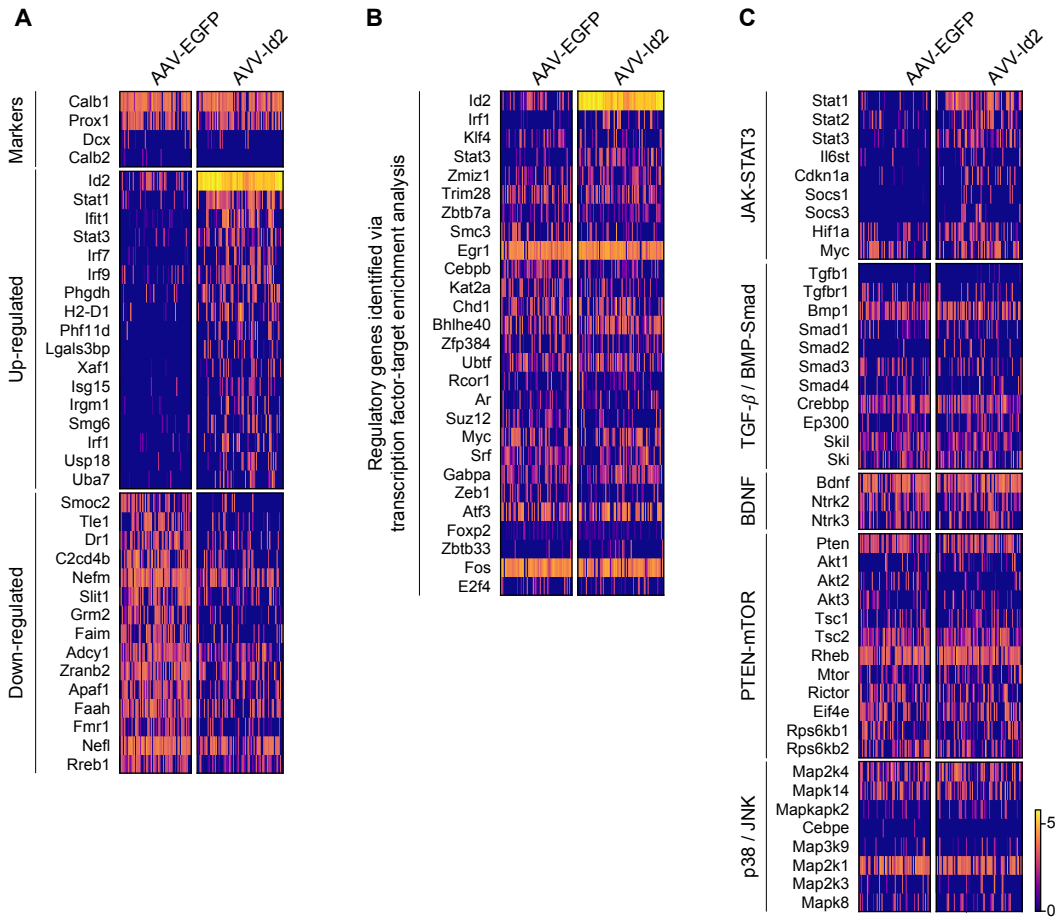

Fig. S5 | AAV-Id2 induced transcriptomic changes in single GCs

(A) Heat map shows the expression of mature (Calb1 and Prox1) and immature (Dcx and Calb2) GC markers, as well as up- and down-regulated genes (from Fig. 5*C*) in single GCs.

(B) Expression of molecules identified using Enrichr transcription factor-target enrichment analysis (from Fig. 5*D*), presumed to interface Id2 and downstream transcriptomic targets.

(C) Expression of genes that belong to the JAK-STAT, TGF-β / BMP-Smad, PTEN-mTOR and p38 / JNK pathways. Scale bar shows $\log_2$-based genes expression level.

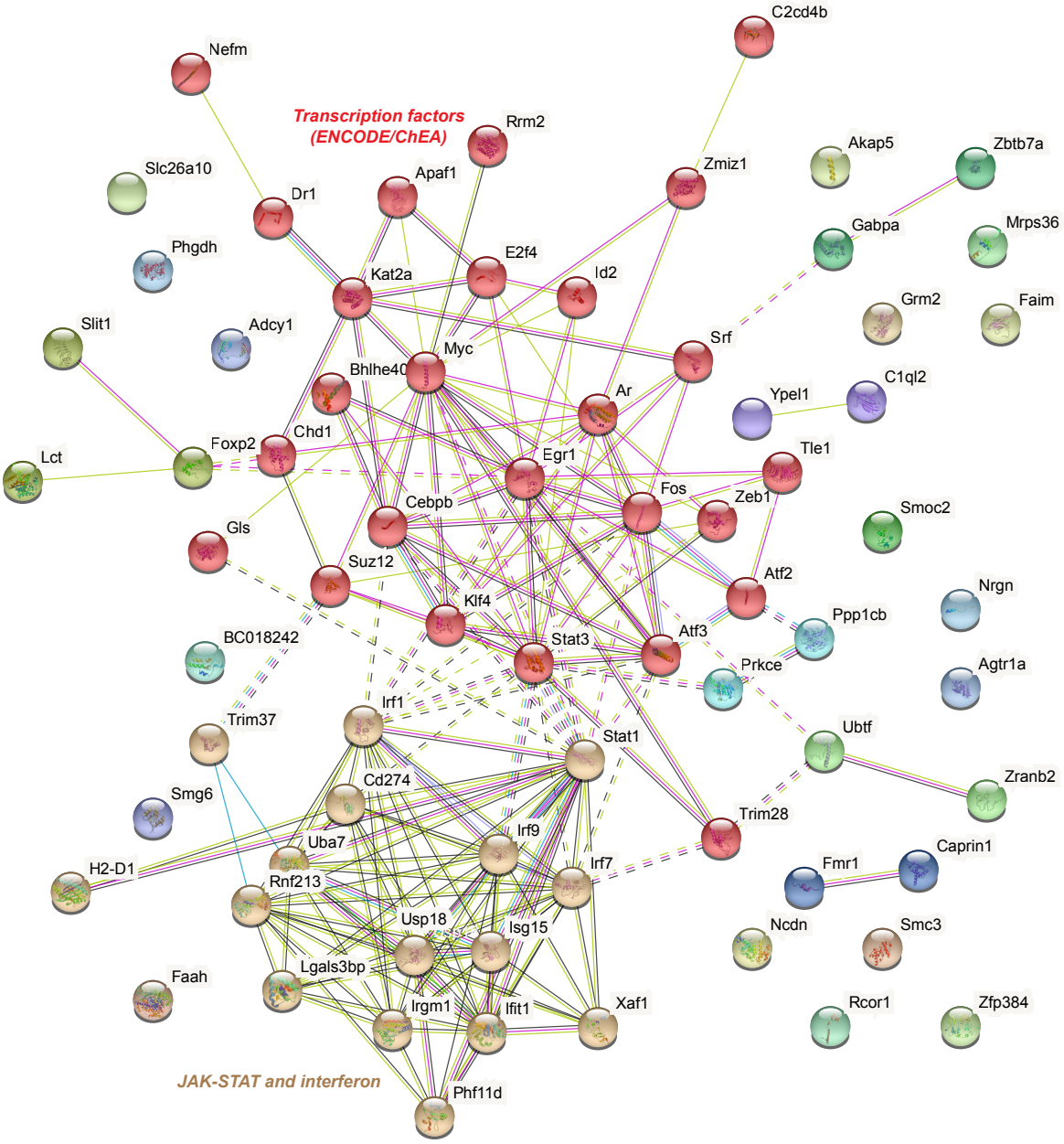

Fig. S6 | STRING based protein-protein interaction map of the gene regulatory network activated by AAV-Id2 Nodes represent proteins identified by differential expression analysis (Fig. 5*C*, FDR<0.05, n=48) and by Enrichr transcription factor-target enrichment analysis (transcription factors; Fig. 5*D*, n=26). Color indicates MCL (Markov Cluster Algorithm) clustering. Edges represent protein-protein association (cyan: from curated databases, magenta: experimentally determined, green: gene neighborhood, blue: gene co-occurrence, light green: textmining, black: co-expression, light blue: protein homology). Inter-cluster edges are represented by dashed-lines.

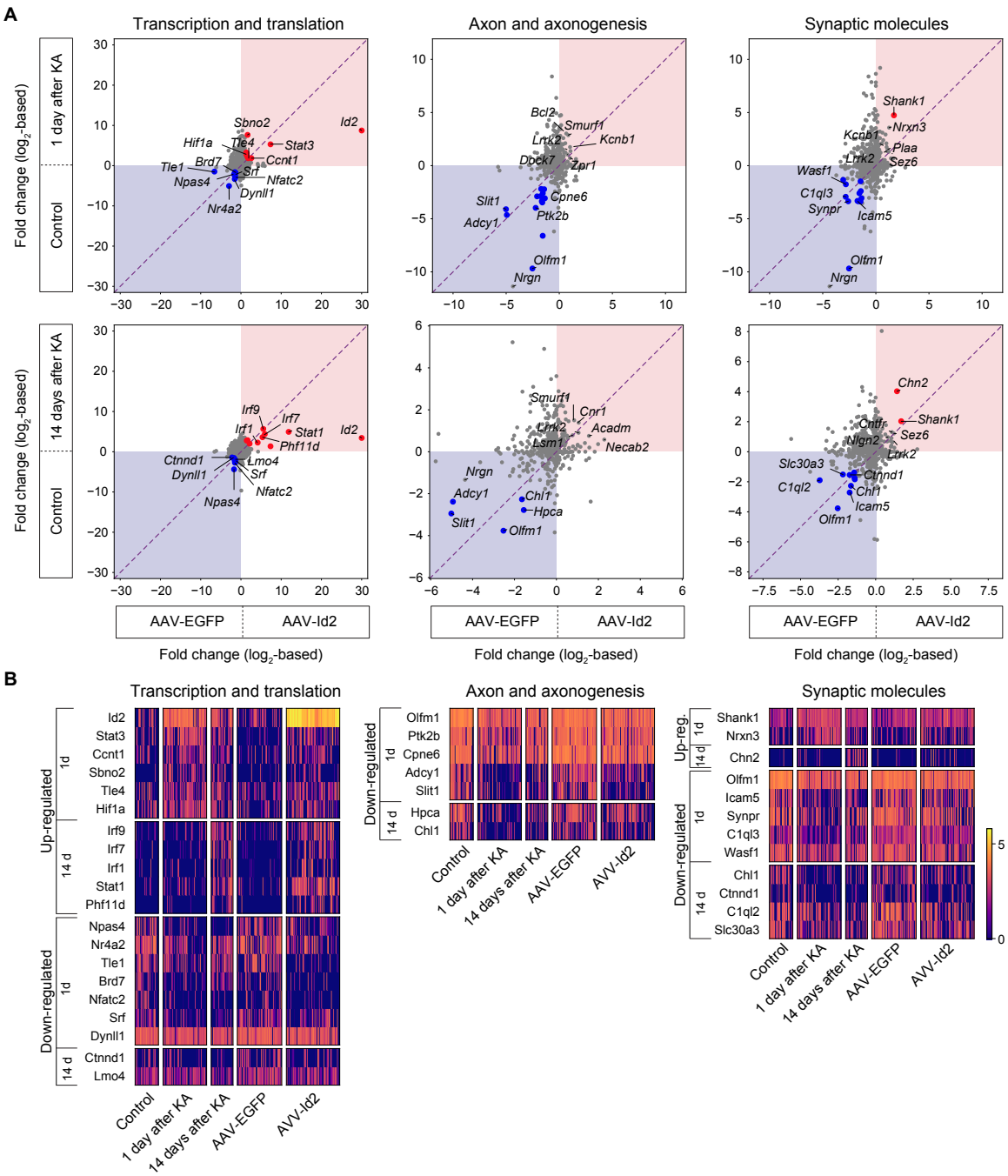

Fig. S7 | Shared transcriptomic changes induced by AAV-Id2 and by KA

(A) Comparison of transcriptomic changes induced by AAV-Id2 (1 month, relative to AAV-EGFP controls) and KA (relative to controls). For each gene, data points represent fold change (log_2(FC)), values in each comparison. Upper panels show regression analysis of AAV-Id2 and 1 day after KA, lower panels show AAV-Id2 and 14 day after KA. From left to right: transcription and translation-related, axon and axonogenesis-related, and synaptic molecules. Molecules in the upper-right (red) and lower-left quadrant (purple) are up- and down-regulated, respectively, both after AAV-Id2 and KA compared to their controls. Highlighted genes were differentially expressed by FDR<0.05 and >2-fold change (or $|log_2FC|>1$ as in plot).

(B) Heat maps show single cell-level expression of top up- and down-regulated genes (highlighted in panel A) as induced by KA and by AAV-Id2. Scale bar shows log_2-based genes expression level.

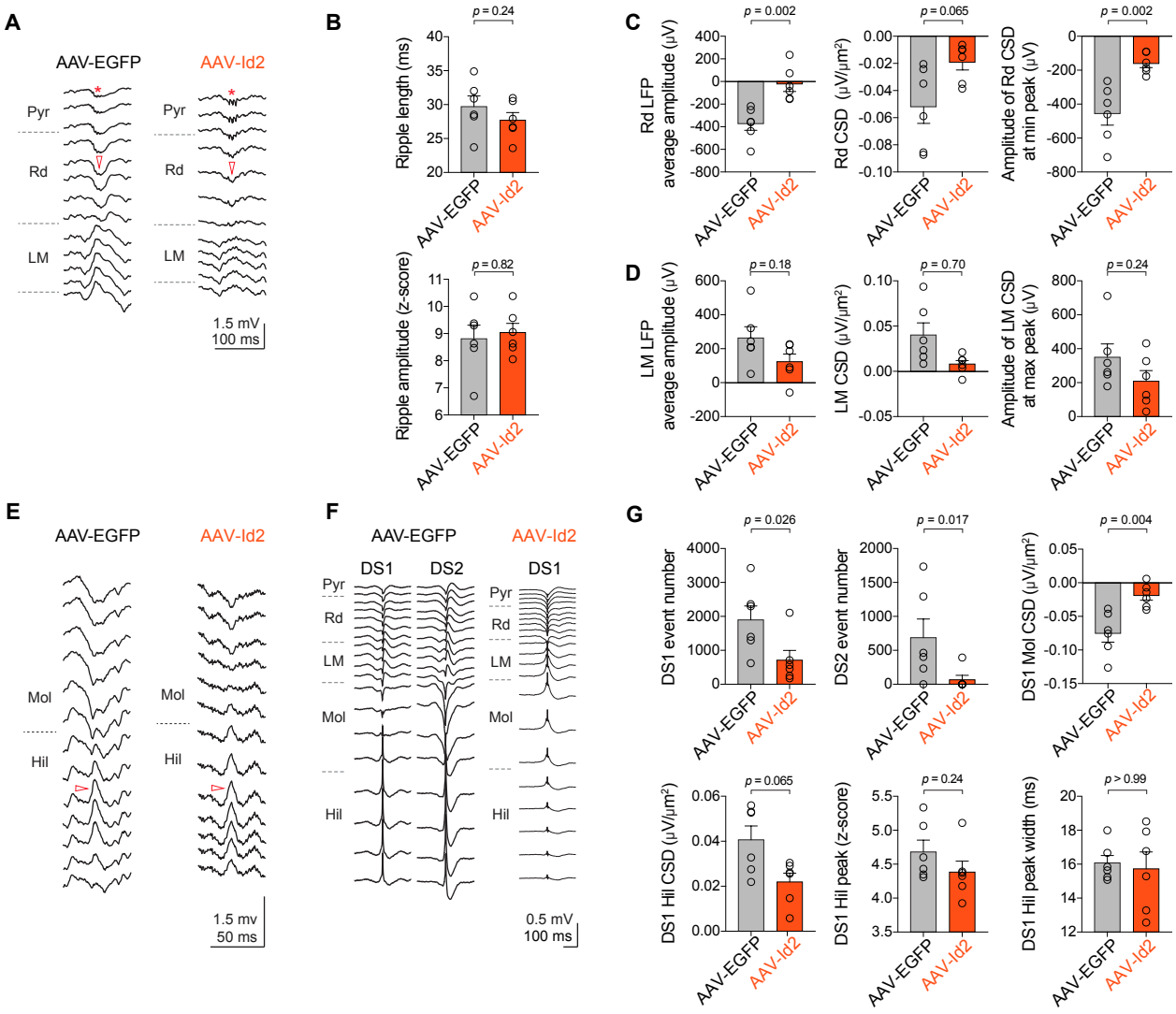

Fig. S8 | In vivo electrophysiological characterization of hippocampal activity after AAV-Id2 delivery
Mice were implanted with linear silicon probes (1 each) into the dorsal hippocampus 8-10 weeks after and recorded while freely moving 3 months after AAV-EGFP (n=6) and AAV-Id2 (n=6) injection.

(A) Example LFP traces recorded from CA1 during immobile, quiet periods 3 months after AAV injections. SWRs are composed of a sharp wave (SW, marked with arrowhead), a large-amplitude negative deflection in radiatum (Rd), and a fast oscillatory ripple pattern (R, marked with asterisk) in pyramidal layer (Pyr).

(B) Quantification of ripple (R) parameters measured in Pyr (Mann-Whitney *U* test).

(C) Quantification of SW parameters measured in radiatum (Rd; Mann-Whitney *U* test).

(D) Quantification of SW parameters measured in lacunosum-moleculare (LM; Mann-Whitney *U* test).

(E) Example LFP traces recorded from dentate gyrus during immobile, quiet periods 3 months after AAV injections. Dentate spikes represent short duration, large-amplitude fluctuation (source) in hilar (Hil) and a corresponding deflection (sink) in molecular layer (Mol) LFPs, marked with arrowhead.

(F) Example type-1 and 2 dentate spike events (DS1 and DS2, respectively).

(G) Quantification of DS1 and DS2 parameters (Mann-Whitney *U* test).

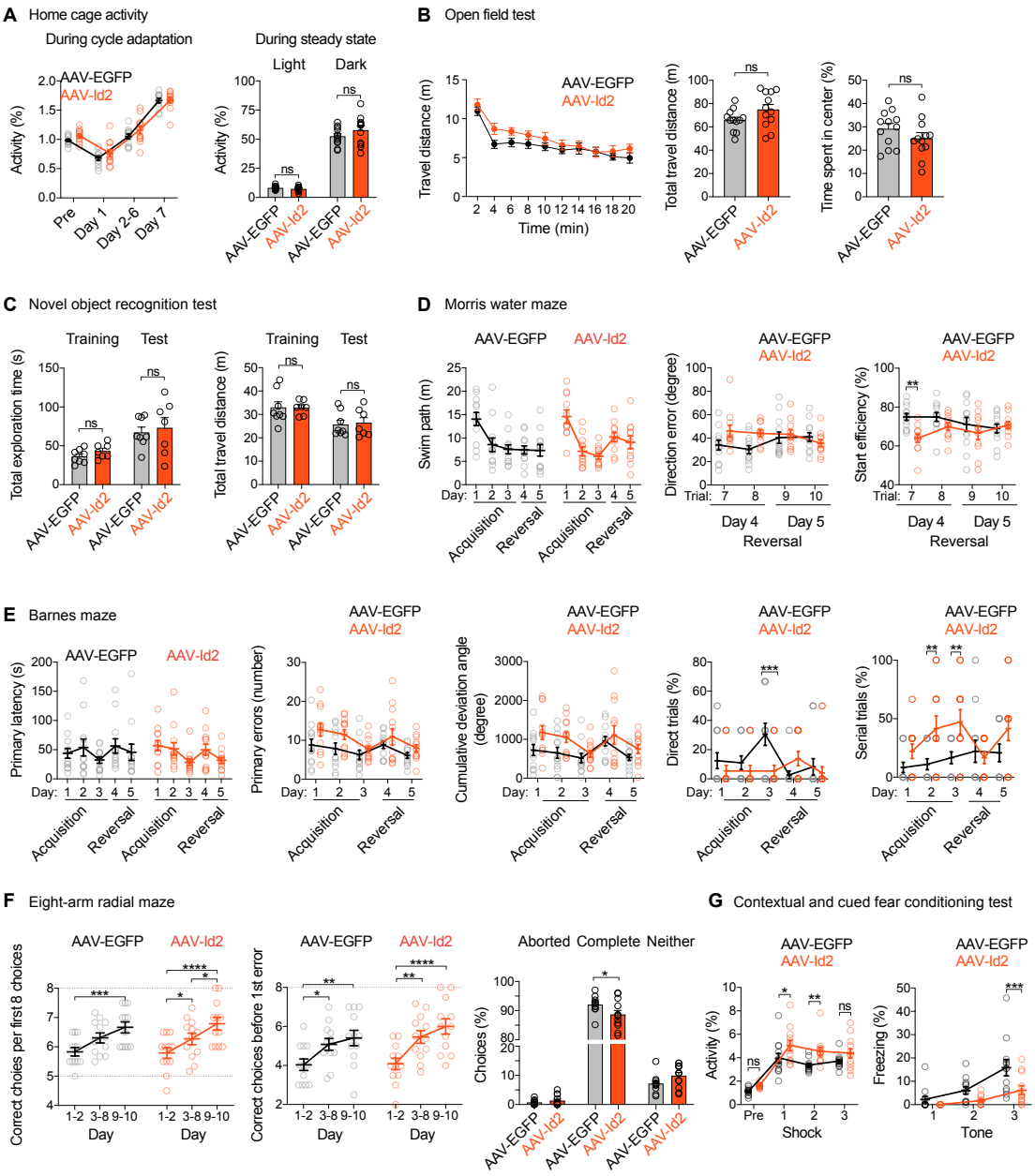

Fig. S9 | Learning and memory after AAV-Id2 induced MF rewiring

(A) Home cage activity. From left to right, plots show activity over days during cycle adaptation (two-way ANOVA: F_{Time} (3,66)=345, p<0.0001; $F_{Treatment}$ (1,22)=1.87, p=0.19; $F_{Treatment\ x\ Time}$ (3, 66)=1.13, p=0.34) and activity on days 9-13 during steady state (two-way ANOVA: F_{Phase} (1,22)=475, p<0.0001; $F_{Treatment}$ (1,22)=1.3, p=0.28; $F_{Treatment\ x\ Phase}$ (1, 22)=2.0, p=0.17; post-hoc analyses: AAV-EGFP vs AAV-Id2: light p=0.74, dark p=0.076).

(B) Open field test. From left to right, plots show travel distance per time segments (two-way ANOVA: F_{Time} (9,198)=23, p<0.0001; $F_{Treatment}$ (1,22)=3.2, p=0.087; $F_{Treatment\ x\ Time}$ (9,198)=0.66, p=0.75), total travel distance (Mann-Whitney *U* test, p=0.10), and time spent in center (Mann-Whitney *U* test, p=0.29).

(C) Novel object recognition test. From left to right, plots show total exploration time (two-way ANOVA: F_{Phase} (1,13)=27, p=0.0002; $F_{Treatment}$ (1,13)=0.5, p=0.49; $F_{Treatment\ x\ Phase}$ (1,13)=0.0076, p=0.93; post-hoc analyses: AAV-EGFP vs AAV-Id2: training p=0.53, test p=0.60) and total travel distance (two-way ANOVA: F_{Phase}

(1,13)=42.51, p<0.0001; $F_{Treatment}$ (1,13)=0.015, p=0.91; $F_{Treatment\ x\ Phase}$ (1,13)=0.13, p=0.72; post-hoc analyses: AAV-EGFP vs AAV-Id2: training p=0.96, test p=0.81).

(D) Morris water maze. From left to right, plots show swim path length over trials (two-way ANOVA, F_{Day} (4,84)=14, p<0.0001; $F_{Treatment}$ (1,21)=0.26, p 0.61; $F_{Treatment\ x\ Day}$ (4,84) =1.4, p=0.23), direction error (two-way ANOVA, $F_{Repetition}$ (3,63)=0.67, p=0.57; $F_{Treatment}$ (1,21)=2.8, p=0.11; $F_{Treatment\ x\ Repetition}$ (3,63)=3.3, p=0.027; post-hoc analyses: trial 7, p=0.026, q=0.063 (does not meet FDR criterion), trial 8, p=0.013, q=0.053 (does not meet FDR criterion), trial 9, p=0.59, trial 10, p=0.34), and start efficiency (two-way ANOVA, $F_{Repetition}$ (3,63)=1.1, p=0.33; $F_{Treatment}$ (1,21)=4.0, p=0.059; $F_{Treatment\ x\ Repetition}$ (3,63)=3.2, p=0.031; post-hoc analyses: trial 7, **p=0.0019, trial 8, p=0.16, trial 9, p=0.20, trial 10, p=0.62).

(E) Barnes maze. From left to right, plots show primary latency (two-way ANOVA, F_{Day} (4,88)=2.6, p=0.042; $F_{Treatment}$ (1,22)=0.096, p=0.76; $F_{Treatment\ x\ Day}$ (4,88)=0.61, p=0.65), primary error (two-way ANOVA, F_{Day} (4,88)=3.6, p=0.0092; $F_{Treatment}$ (1, 22)=8.8, p=0.0072; $F_{Treatment\ x\ Day}$ (4,88)=0.39, p=0.82; post-hoc analyses: AAV-EGFP vs AAV-Id2, day 1, p=0.037, q=0.13 (does not meet FDR criterion), day 2, p=0.053, q=0.13 (does not meet FDR criterion), day 3, p=0.47, day 4, p=0.27, day 5, p=0.32), cumulative deviation angle (two-way ANOVA, F_{Day} (4,88)=4.0, p=0.0046; $F_{Treatment}$ (1,22)=7.2, p=0.013; $F_{Treatment\ x\ Day}$ (4,88)=0.59, p=0.66; post-hoc analyses: AAV-EGFP vs AAV-Id2, day 1, p=0.028, q=0.12 (does not meet FDR criterion), day 2, p=0.048, q=0.12 (does not meet FDR criterion), day 3, p=0.59, day 4, p=0.44, day 5, p=0.28), direct trials (two-way ANOVA, F_{Day} (4,88)=1.9, p=0.12; $F_{Treatment}$ (1,22)=3.6, p=0.070; $F_{Treatment\ x\ Day}$ (4,88)=3.6, p=0.0091; post-hoc analyses: AAV-EGFP vs AAV-Id2, day 1, p=0.31, day 2, p=0.42, day 3, ***p=0.0004, day 4, p=0.11, day 5, p=0.54), and serial trials (two-way ANOVA, F_{Day} (4,88)=2.4, p=0.053; $F_{Treatment}$ (1,22)=6.3, p=0.02; $F_{Treatment\ x\ Day}$ (4,88)=2.5, p=0.046; post-hoc analyses: AAV-EGFP vs AAV-Id2, day 1, p=0.21, day 2, **p=0.0067, day 3, **p=0.0067, day 4, p=0.62, day 5, p=0.062).

(F) Eight-arm radial maze. From left to right, plot shows correct choices (number of baits) per first 8 choices (two-way ANOVA, F_{Day} (2,44)=17, p<0.0001; $F_{Treatment}$ (1,22)=0.0077, p=0.93; $F_{Treatment\ x\ Day}$ (2,44) =0.18, p=0.83; post-hoc analyses: AAV-EGFP: days 1-2 vs 9-10, ***p=0.0004; AAV-Id2: days 1-2 vs 3-8, *p=0.034, days 1-2 vs 9-10, ****p<0.0001, days 3-8 vs 9-10, *p=0.022), correct choices before 1st error (two-way ANOVA, F_{Day} (2,44)=17, p 0.0001; $F_{Treatment}$ (1,22)=0.97, p=0.34; $F_{Treatment\ x\ Day}$ (2,44) =0.45, p=0.64; post-hoc analyses: AAV-EGFP: days 1-2 vs 3-8, *p=0.014, days 1-2 vs 9-10, **p=0.0016; AAV-Id2: days 1-2 vs 3-8, **p=0.0015, days 1-2 vs 9-10, p 0.0001), and proportion of different types of choices (two-way ANOVA, F_{Type} (2,44)=3922, p<0.0001; $F_{Treatment}$ (1,22)=0.0, p>1; $F_{Treatment\ x\ Type}$ (2,44) =4.0, p=0.026; post-hoc analyses: AAV-EGFP vs AAV-Id2, aborted, p=0.62, complete, *p=0.01, neither, p=0.035, q=0.0529 (does not meet FDR criterion).

(G) Contextual and cued fear conditioning test. From left to right, plots show percentage activity before (pre) and during training shocks (two-way ANOVA, F_{Phase} (3,66)=77, p<0.0001; $F_{Treatment}$ (1,22)=7.7, p=0.011; $F_{Treatment\ x\ Phase}$ (3,66) =1.1, p=0.35; post-hoc analyses: AAV-EGFP vs AAV-Id2: pre, p=0.27, 1st shock, *p=0.010, 2nd shock, **p=0.0053, 3rd shock, p=0.10), and freezing to tone during training (CS; two-way ANOVA, F_{Phase} (2,44)=8.0, p<0.0001; $F_{Treatment}$ (1,22)=7.6, p=0.0013; $F_{Treatment\ x\ Phase}$(2,44)=3.3, p=0.044; post-hoc analyses: AAV-EGFP vs AAV-Id2: 1st tone p=0.40, 2nd tone p=0.095, 3rd tone, ***p=0.0004).

Table S1. Statistical analyses related to main figures

Figure	Description and statistical analysis
Figure 2D	Quantification of total axon length after AAV-EGFP and AAV-Id2 injections
	One-way ANOVA, F=15, p=0.0001, post-hoc analyses: AAV-EGFP vs AAV-Id2, 1 month, *p=0.043; 2 months, *p=0.023; 3 months, ****p<0.0001.
Figure 2E	Quantification of Timm's positive puncta size in GCL/IML after AAV-EGFP, and 1, 2, and 3 months after AAV-Id2 injections
	Two-way ANOVA, F_{Area} (1,9)=32, p=0.0003; $F_{Treatment}$ (3,9)=26, p<0.0001; $F_{Area\ x\ Treatment}$ (3,9)=14, p=0.0009; post-hoc analyses: GCL: AAV-EGFP vs AAV-Id2, 1 month, ***p=0.0003; 2 months, ****p<0.0001; 3 months, ****p<0.0001. IML: AAV-EGFP vs AAV-Id2, 1 month, p=0.053; 2 months, ****p<0.0001; 3 months, ****p<0.0001.
Figure 2G	Quantification of ZnT3-positive puncta density in GCL/IML 3 months after AAV-EGFP and AAV-Id2 injections
	Two-way ANOVA, F_{Area} (1,17)=0.068, p=0.80; $F_{Treatment}$ (1,17)=44, p<0.0001; $F_{Area\ x\ Treatment}$ (1,17)=1.1, p=0.30; post-hoc analyses: GCL: AAV-EGFP vs AAV-Id2, ****p<0.0001; IML: AAV-EGFP vs AAV-Id2, ****p<0.0001.
Figure 2H	Quantification of ZnT3-positive puncta size in GCL/IML 3 months after AAV-EGFP and AAV-Id
	Two-way ANOVA, F_{Area} (1,8)=5.9, p=0.044; $F_{Treatment}$ (1,8)=8.7, p=0.019; $F_{Area\ x\ Treatment}$ (1,8)=5.7, p=0.044; post-hoc analyses: GCL: AAV-EGFP vs AAV-Id2, **p=0.0022; IML: AAV-EGFP vs AAV-Id2, p=0.089.
Figure 3E	Quantification Timm's staining intensity. Intensities were measured relative to signals in the hilus of the same sections
	Two-way ANOVA, F_{Area} (1,11)=29, p=0.0002; $F_{Treatment}$ (1,11)=42, p<0.0001; $F_{Area\ x\ Treatment}$ (1,11)=5.1, p=0.045; post-hoc analyses: GCL: Control vs AAV-Id2, **p=0.0017; IML: Control vs AAV-Id2, ****p<0.0001.
Figure 4D	Amplitude of light-evoked EPSC amplitude in GCs of dorsal hippocampus
	Mann-Whitney *U* test, *p=0.048.
Figure 4E	Amplitude of light-evoked EPSC amplitude in GCs of ventral hippocampus
	Mann-Whitney *U* test, **p=0.0075.
Figure 6C	LFP power of delta, theta, beta, slow gamma, mid gamma, fast gamma (all during locomotion), and ripple and fast ripple (during resting) range frequencies (AAV-EGFP, n=7 mice; AAV-Id2, n=6 mice).

Figure	Description and statistical analysis
	• Delta: two-way ANOVA, F_{Layers} (4,38)=11, p<0.0001; $F_{Treatment}$ (1,10)=0.095, p=0.76; $F_{Treatment\ x\ Phase}$ (4,38)=0.30, p=0.88, • theta: F_{Layers} (4,38)=14, p<0.0001; $F_{Treatment}$ (1,10)=0.069, p=0.94; $F_{Treatment\ x\ Phase}$ (4,38)=0.49, p=0.75, • beta: F_{Layers} (4,38)=10, p<0.0001; $F_{Treatment}$ (1,10)=1.3, p=0.28; $F_{Treatment\ x\ Phase}$ (4,38)=0.37, p=0.83 • slow gamma: F_{Layers} (4,38)=12, p<0.0001; $F_{Treatment}$ (1,10)=0.05, p=0.82; $F_{Treatment\ x\ Phase}$ (4,38)=1.4, p=0.26, • mid gamma: F_{Layers} (4,38)=11, p<0.0001; $F_{Treatment}$ (1,10)=1.5, p=0.25; $F_{Treatment\ x\ Phase}$ (4,38)=1.8, p=0.16, • fast gamma: (F_{Layers} (4,38)=11, p<0.0001; $F_{Treatment}$ (1,10)=1.0, p=0.33; $F_{Treatment\ x\ Phase}$ (4,38)=0.90, p=0.47, • ripple: F_{Layers} (4,38)=10, p<0.0001; $F_{Treatment}$ (1,10)=0.66, p=0.44; $F_{Treatment\ x\ Phase}$ (4,38)=0.50, p=0.73, • fast ripple: F_{Layers} (4,38)=7.8, p=0.0001; $F_{Treatment}$ (1,10)=0.31, p=0.59; $F_{Treatment\ x\ Phase}$ (4,38)=0.75, p=0.56.
Figure 6D	Quantification of ripple occurrence and intra-ripple frequency in CA1 Pyr and Rd (AAV-EGFP, n=6 mice; AAV-Id2, n=6 mice).
	• Ripple occurrence: Mann-Whitney *U* test, p=0.31, • intra-ripple frequency: Mann-Whitney *U* test, p=0.45.
Figure 6E	Quantification of DS1 and DS2 occurrence (AAV-EGFP, n=6 mice; AAV-Id2, n=6).
	• DS1 occurence: Mann-Whitney *U* test, p=0.065, • DS2 occurence: Mann-Whitney *U* test, p=0.015.
Figure 7A	Quantification of discrimination index (DI) in novel object recognition test.
	Two-way ANOVA, F_{Phase} (1,13)=95, p<0.0001; $F_{Treatment}$ (1,13)=4.7, p=0.050; $F_{Treatment\ x\ Phase}$ (1,13)=2.1; post-hoc analyses: AAV-EGFP vs AAV-Id2, training p=0.87, test *p=0.021.
Figure 7B	Quantification of alteration and choice latency in T maze test.
	• Alteration: Mann-Whitney *U* test, p=0.33, • choice latency: two-way ANOVA, $F_{Repetition}$ (5,100)=6.0, p<0.0001, $F_{Treatment}$ (1,20)=11, p=0.0036; $F_{Treatment\ x\ Repetition}$ (5,100) =4.2, p=0.0018; post-hoc analyses: AAV-EGFP vs AAV-Id2, trial 1, p=0.87, trial 2, p=0.66, trial 3, p=0.31, trial 4, **p=0.0048, trial 5, *p=0.011, trial 6, ****p<0.0001.
Figure 7C	Quantification of escape latency, quadrant time, swim path length parallel to border walls, and the number of wall approaches in Morris water maze.
	• Escape latency: two-way ANOVA, F_{Day} (4,84)=13, p<0.0001; $F_{Treatment}$ (1, 21)=0.056, p=0.82; $F_{Treatment\ x\ Day}$ (4,84) =1.4, p=0.23), • quadrant time: 1st probe trial, two-way ANOVA, F_{Place} (1,21)=14, p=0.0013; $F_{Treatment}$ (1,21)=1.8, p=0.19; $F_{Treatment\ x\ Place}$ (1,21)=0.018, p=0.90; post-hoc analyses: AAV-EGFP: adjacent vs target, *p=0.017; AAV-Id2: adjacent vs target, *p=0.014; 2nd probe trial, two-way ANOVA, F_{Place} (1,21)=6.9, p=0.016; $F_{Treatment}$ (1,21)=6.9, p=0.016; $F_{Treatment\ x\ Place}$ (1,21)=5.3, p=0.031; post-hoc analyses: AAV-EGFP: adjacent vs target, p=0.82; AAV-Id2: adjacent vs target, **p=0.0026, • swim path length parallel to border walls: two-way ANOVA, F_{Phase} (1,21)=3.3, p=0.082; $F_{Treatment}$ (1,21)=0.99, p=0.33; $F_{Treatment\ x\ Phase}$ (1,21)=8.6, p=0.008, post-hoc analyses: AAV-EGFP: acquisition vs reversal, **p=0.0025; AAV-Id2: acquisition vs reversal, p=0.45, • number of wall approaches: two-way ANOVA, F_{Phase} (1,21)=2.6, p=0.12; $F_{Treatment}$ (1,21)=0.67, p=0.42; $F_{Treatment\ x\ Phase}$ (1,21)=6.0, p=0.023; post-hoc analyses: AAV-EGFP: acquisition vs reversal, **p=0.0079; AAV-Id2: acquisition vs reversal, p=0.57.

Figure	Description and statistical analysis
Figure 7D	Quantification of primary path length, primary errors, poke ratio in probe trial after acquisition, and average strategy used during acquisition and reversal training in Barnes maze.
	• Primary path length: two-way ANOVA, F_{Day} (4,88)=6.6, p=0.0001; $F_{Treatment}$ (1,22)=0.4, p=0.52; $F_{Treatment\ x\ Day}$ (4,88) =0.3, p=0.85, • primary errors: Mann-Whitney *U* test, **p=0.0038, poke ratio in probe trial after acquisition: two-way ANOVA, F_{Degree} (7,88)=6.2, p=0.0002; $F_{Treatment}$ (1,22)=5.0, p=0.035; $F_{Treatment\ x\ Degree}$ (4,88)=4.3, p=0.003; post-hoc analyses: angle=0˚: AAV-EGFP vs AAV-Id2, ****p<0.0001, • average strategy used during acquisition and reversal training: two-way ANOVA, $F_{Strategy}$ (2,44)=59, p<0.0001; $F_{Treatment}$ (1,22)=1.3, p=0.28; $F_{Treatment\ x\ Degree}$ (2, 44)=4.4, p=0.018; post-hoc analyses: AAV-EGFP vs AAV-Id2: direct, p=0.31, serial, **p=0.0047, mixed p=0.059.
Figure 7E	Quantification of memory errors (i.e. entry to an arm where bait was already consumed) per consumed baits over days, memory error per consumed bait, preferred angle, and choice performed at preferred angle in eight-arm maze.
	• Memory errors per consumed baits over days: two-way ANOVA, F_{Day} (2,44)=9.0, p=0.0005; $F_{Treatment}$ (1,22)=2.8, p=0.11; $F_{Treatment\ x\ Day}$ (2,44)=0.53, p=0.59, • memory error per consumed bait: two-way ANOVA, F_{Bait} (2,44)=148, p<0.0001; $F_{Treatment}$ (1,22)=2.8, p=0.11; $F_{Treatment\ x\ Bait}$ (2,44)=3.5, p=0.041; post-hoc analyses: AAV-EGFP vs AAV-Id2: bait 1-4, p=0.88, bait 5-6, p=0.86, bait 7-8, **p=0.0029, • preferred angle: two-way ANOVA, F_{Angle} (2,44)=16, p<0.0001; $F_{Treatment}$ (1,22)=0.056, p=0.81; $F_{Treatment\ x\ Angle}$ (2,44)=2.6, p=0.086, • choice performed at preferred angle: two-way ANOVA, F_{Day} (2,44)=16, p<0.0001; $F_{Treatment}$ (1,22)=0.056, p=0.81; $F_{Treatment\ x\ Day}$ (2,44) =2.6, p=0.086; post-hoc analyses: AAV-EGFP, days 1-2 vs 3-8, **p=0.0071, days 1-2 vs 9-10, *p=0.020, day 3-8 vs 9-10, p=0.68; AAV-Id2, days 1-2 vs 3-8, **p=0.0049, days 1-2 vs 9-10, ****p<0.0001, days 3-8 vs 9-10, *p=0.026.
Figure 7F	Quantification of freezing during context retention test, freezing during cue retention test, and freezing during extinction test in contextual and cued fear conditioning test.
	• Freezing during context retention test: two-way ANOVA, F_{Phase} (1,22)=73, p<0.0001; $F_{Treatment}$ (1,22)=19, p=0.0003; $F_{Treatment\ x\ Phase}$ (1,22)=14, p=0.0012; post-hoc analyses: AAV-EGFP vs AAV-Id2: baseline, p=0.60, context, ****p<0.0001, • freezing during cue retention test: two-way ANOVA, F_{Phase} (1,22)=46, p<0.0001; $F_{Treatment}$ (1, 22)=3.4, p=0.080; $F_{Treatment\ x\ Phase}$ (1,22) =1.6, p=0.22; post-hoc analyses: AAV-EGFP vs AAV-Id2: pre-tone, p=0.58, tone, p=0.032, q=0.064 (does not meet FDR criterion), • freezing during extinction test: two-way ANOVA, F_{Phase} (2,44)=15, p<0.0001; $F_{Treatment}$ (1, 22)=1.3, p=0.27; $F_{Treatment\ x\ Phase}$(2,44)=0.25, p=0.78; post-hoc analyses: AAV-EGFP vs AAV-Id2: Baseline, p=0.24, 1st tone, p=0.38, last tone, p=0.73.

Materials and methods

Mouse breeding and husbandry

All mouse protocols and husbandry practices were approved by the Veterinary Office of Zürich Kanton. The University of Zurich animal facilities comply with all appropriate standards (cages, space per animal, temperature, light, humidity, food, water) and all cages were enriched with materials that allow the animals to exert their natural behavior. Animals were housed under a 12-12 hour light-dark cycle. The following lines were used in this study (*1*) Calb1-IRES2-Cre-D: B6;129S-Calb1tm2.1(cre)Hze/J (JAX:028532), (*2*) Rbp4-Cre: Tg(Rbp4-cre)KL100Gsat/Mmucd/MMRRC:031125. Animals were backcrossed by at least five generations to C57BL/6J. All animals were aged from 2 to 5 months, age-matched and underwent the same surgical procedures. Both males and females were used for histological, transcriptomic and electrophysiological analyses. Only males were used for in vivo electrophysiology and behavior.

Plasmids and viruses

Mouse Id2 gene was amplified from mouse brain total RNA (Clontech, #636601; coding sequences were identical to NCBI ACCESSION NM_010496.3), cloned into Cre-dependent gene expression vector and packaged into adeno-associated virus serotype DJ/8 (vWL40.AAVDJ8/2-shortCAG-dlox-mId2(rev)-dlox-WPRE, 1.9×10^{13} vg/ml), which we refer to as AAV-Id2 for short. For control experiments, Cre-dependent EGFP virus (v217.AAVDJ8/2-hEF1a-dlox-EGFP(rev)-dlox-WPRE-bGHp(A), 5.3×10^{12} vg/ml) was used, which we refer to as AAV-EGFP. For Cre-independent wild-type and mutant Id2 expression experiments, AAV.CaMKIIα-Id2 (vWL85.AAVDJ8/2-mCaMKIIα-mId2_FLAG-WPRE, 4.2×10^{13} vg/ml) and AAV.CaMKIIα-Id2 mutant (S14A) (vWL84.DJ8 /2-mCaMKIIα-mId2(S14A)_FLAG-WPRE, 5.3×10^{13} vg/ml) were used. For ChR expression, v80.AAV5-hEF1a-dlox-hChR2(H134R)_mCherry(rev)-dlox-WPRE (9.1×10^{12} vg/ml) was used, which we refer to as AAV-ChR-mCherry. All viral vectors were produced by the Viral Vector Facility (VVF) of the Neuroscience Center Zurich (ZNZ).

Stereotactic injection

Mice were deeply anesthetized and placed into a stereotactic apparatus. Microinjections were performed at a rate of 100 nl/min using a programmable syringe pump with 35-gauge beveled NanoFil needle (World Precision Instruments, USA). Injection coordinates for targeting dorsal dentate gyrus: -1.9 mm anterior/posterior, 1.2 mm middle/lateral, -1.8 mm ventral/dorsal to bregma; for ventral dentate gyrus: -3.4 mm anterior/posterior, 2.9 mm middle/lateral, -3.3 mm ventral/dorsal to bregma. Injection details are summarized as follow:

(1) KA microinjection: For histological characterization, 2-month-old C57BL/6J mice were unilaterally injected with 70 nl 5 mM kainic acid (KA) in saline solution into ventral dentate gyrus. For controls, only saline injection was used.

(2) In vitro electrophysiology and single-cell RNAseq after KA: GCs were collected from 1-2 month old mice 1 (70 nl 5 mM KA, unilateral) and 14 days after KA (mixture of 70 nl 5 mM KA and 70 nl v24.AAV5/2-CAG-EGFP-WPRE 4.1×10^{12} vg/ml, where EGFP expression was used to confirm injection position, bilateral). For controls, 1 month-old non-injected animals were used.

(3) AAV delivery of EGFP and Id2: For histological characterization, brain slice electrophysiology, single-cell morphological reconstruction, electron microscopy characterization and patch-RNAseq, 2 to 3-month-old Calb1-IRES2-Cre-D mice were injected with 500 nl of a mixture containing equal volume of AAV-Id2 and AAV-EGFP. For controls, mice were injected with 500 nl PBS-diluted AAV-EGFP (equal volume dilution). For Cre-independent wild-type and mutant Id2 expression experiments, 3 month-old wild-type mice were injected with 500 nl AAV.CaMKIIα-Id2 and AAV.CaMKIIα-Id2(S14A) respectively.

(4) In vitro electrophysiology: For ChR experiments, 2 to 3-month-old Rbp4-Cre mice were injected with a mixture of virus containing equal volume of AAV-Id2 and AAV-ChR-mCherry. Control mice were injected with only AAV-ChR-mCherry diluted with equal volume of PBS.

(5) In vivo electrophysiology: Viral injections were done as described in *(3)*, but injections were bilateral, and targeted both dorsal and ventral hippocampus. In each animal, 500 nl viral mixture was injected in each of the four position (in total, 2000 nl of viral mixture were injected).

Single-cell RNA sequencing and bioinformatics

Sample collection and library preparation were as previously described (1) with the following modifications: single-cell mRNA was processed using Clontech's SMARTer Ultra Low RNA Input v4 or SMART-Seq HT kit and pooled libraries were sequenced using NextSeq 300 high-output kit on an Illumina NextSeq 500 System with 2x75 paired-end reads.

(1) Processing of RNAseq data: After sequencing, raw reads were de-multiplexed and pre-processed using Trimmomatic and Flexbar. Then, reads were aligned to the Ensembl GRCm38 reference transcriptome (Version-86), using the STAR aligner with the following parameters: trimLeft = 10, minTailQuality = 15, minAverageQuality = 20 and minReadLength = 30. 'Single-end/paired-end' and 'sense/antisense/both' options were used. Gene counts were calculated using HTSeq. For convenience, Ensembl gene IDs were converted to gene symbols using the mouse GRCm38 gtf file (ftp://ftp.ensembl.org/pub//release-86/gtf/mus_musculus/Mus_musculus.GRCm38.86.gtf.gz) as a reference. In the few cases where different Ensembl gene IDs identified the same gene symbol, total gene counts were used.

(2) Quality control: All data analysis was performed using Python codes. First, in each cell, we calculated the number of unique genes, nuclear genes, and mitochondrial genes. Second, we calculated the median and median absolute deviation of the $\log_{10}$ of these values across all cells. Cells that had any of the three values more than 3 median absolute deviations below the median were removed as failing quality control.

(3) Normalization of gene expression: Scran with sizes of 10, 20, 30, 40, and 50 was used to normalize cells against each other. Cells with a size factor of 0 or less were removed as an extra step of quality control.

(4) Differential gene expression: First, we performed a $\log_2$ transformation of our data with a pseudocount of 1 to handle 0 expression ($y = \log_2(1+x)$). Second, as feature selection, genes that did not have an expression higher than 0.1 in at least 10 cells were removed. Then, for the remainder of the genes, we performed the Welch's t-test and the fold change (FC) in the transformed expressions to calculate the p-value and $\log_2(FC)$, respectively. Benjamini and Hochberg method was used to correct for multiple testing (FDR). Genes with >2-fold change ($|\log_2 FC|>1$) in average expression and FDR<0.05 were considered significantly differently expressed. In *SI Appendix*, Fig. S1 and S7, the following gene lists were used: Transcription and translation (GO:0010467); Axon and axonogenesis (GO:00340424, GO:0033267, GO:0007409, GO:0050771, GO:0050772, GO:0007411, Nefm was manually added); Synaptic molecules (GO:0099003 and cell-adhesion molecules as previously defined in Ref. 1).

(5) Transcription factor-target enrichment: Enrichr (https://maayanlab.cloud/Enrichr/) was run with p-value<0.05 up- (n=285) and down-regulated (n=848) genes using ENCODE (Encyclopedia of DNA elements project) and ChEA (Chip=X enrichment Analysis) options. Genes that had an expression level >0.1 in at least 30% of GCs in either AAV-EGFP or AAV-Id2 conditions, and a combined Enrichr score >1 were included in Fig. 5D.

(6) Protein-Protein interaction networks: SRTING (Functional protein association networks, version 11.0; https://string-db.org) was run using differentially expressed genes (FDR<0.05, n=48) and Enrichr identified transcription factors (n=26) as input. Markov Cluster Algorithm (MCL, inflation parameter=1.6) was applied to cluster proteins in the network.

Histology and neuroanatomy

(1) Sample preparation: Animals were deeply anesthetized and transcardially perfused first with with 3 ml 0.9% saline solution followed by 3 ml 0.1% Na_2S in 0.1M PB solution, and then by 4% paraformaldehyde (PFA) in 0.1 M PB (1ml/1g bodyweight). Brains were immersed into 4% PFA in 0.1 M PB overnight at 4 °C and then sectioned next day using a vibratome, or further transferred into 30% sucrose in 0.1 M PB and stored at 4 °C until sectioning using a frozen tissue sliding microtome. Fixed brains were cut into 50 or 80 µm thick horizontal or coronal sections.

(2) Immunohistochemistry: Slices were first permeabilized and blocked in incubating medium (0.1M PB containing 5% normal goat serum and 0.2% Triton) for 1 hour at room temperature, and then incubated overnight with primary antibodies at 4 °C. Primary antibodies used: Rabbit monoclonal anti-SLC30A3 (ZnT3; ThermoFisher, PA5-77769, 1:600), Guinea pig polyclonal ZnT3 antiserum (Synaptic system, #197004, 1:500), Rabbit polyclonal anti-ID2, (Abcam, ab52093, 1:50). Next day, slices were rinsed in 0.1 M PB and incubated with secondary antibodies overnight at 4 °C. Secondary antibodies: Goat anti-Rabbit IgG (H+L) Cross-Adsorbed, Alexa Fluor 488 (Invitrogen, A-11008, 1:500), Goat anti-Rabbit IgG (H+L) Cross-Adsorbed, Alexa Fluor 568 (Invitrogen, A-11011, 1:500), anti-Guinea Pig IgG (H+L) Highly Cross-Adsorbed Secondary Antibody, Alexa Fluor 568 (Invitrogen, A-11075, 1:500). Sections were rinsed in 0.1 M PB (some sections were subsequently stained with DAPI for nuclear staining) and mounted in Vectashield (Vector Laboratories) for analysis. Fluorescent images were acquired using a Leica SP8 Confocal Laser Scanning Microscope. Image analysis were performed using Fiji/ImageJ.

(3) Timm's staining and axon tracing: Sections were rinsed in 0.1 M PB and post-fixed in 2.5% glutaraldehyde in 0.1 M PB solution for 10 min. Then, sections were rinsed in 0.1 M PB and immersed in Timm's reaction solutions, a 12:6:2 mixture of 20% gum arabic, hydroquinone and citric acid trisodium citrate buffer, with 100 µl of 17% silver nitrate solution. The reaction was carried out for 20 to 30 min at 29 °C, then slices were washed thoroughly in 0.1M PB. After dehydration steps, the sections were mounted using DPX mounting medium and imaged using a wide-field microscope. Stained axons in dentate gyrus were traced using „Simple neurite tracer" of Fiji/ImageJ.

(4) Single cell reconstruction: Biocytin-filled cell-containing brain slices were fixed 4% PFA in 0.1 M PB overnight at 4 °C. Next day, after DAB staining (Vectastain ABC KIT, Vector Laboratories), sections were dehydrated and mounted in DPX mounting medium (Electron Microscopy Science, UK). Cells were reconstructed with Neurolucida (MicroBrightField, Inc., USA).

Electron microscopy

Animals were deeply anesthetised and transcardially perfused first with saline and then with 2% PFA and 0.1% glutaraldehyde dissolved in 0.1M Na-acetate buffer (pH 6) for 5 minutes, followed by 30-40 minutes with 2% PFA and 0.1% glutaraldehyde dissolved in 0.1M Na-borate buffer (pH 8.5). Brains were sectioned horizontally into 60 µm thin sections with a vibratome. Sections were incubated for 48 hours at 8 °C in polyclonal rabbit ZnT3 antiserum (Synaptic Systems, Germany, catalogue #197002, 1:5000) diluted in 0.1 M PB. After extensive washes sections were incubated for 8 hours in biotinylated donkey-anti-rabbit (711-065-152, 1:500; Jackson Immunoresearch) solution at room temperature. Sections were developed with standard avidin-biotin peroxidase kit (1:500; Vectastain) and diamino-benzidine (DAB, Sigma-Aldrich) was used as a chromogen. After treatment with 1% Osmium-tetroxide (SPI Supplies) and 1% Uranyl-acetate (Amersham), slices were dehydrated and embedded in durcupan (Sigma-Aldrich). 60 nm ultrathin sections were contrasted with 3% Lead citrate (Leica) and imaged using a Jeol JEM 1400-Plus transmission electron microscope. For tomography 150-180 nm thin serial sections were used without Lead citrate contrasting. Single-axis tilting was performed in a range of 120 with single steps. Images were taken with 30k magnification. 3D rendering was performed with Amira (2020.1, Thermo Fisher Scientific). Digital images were brightness/contrast adjusted with ImageJ.

In vitro electrophysiology

Brain slice preparation, recording solutions, whole cell patch-clamp recording, and measurement of biophysical properties were as as previously described (2). Cells were visualized by infrared differential interference contrast optics in an upright microscope (Olympus; BX-51WI) using Hamamatsu Orca-Flash 4.0 CMOS camera, and recorded using borosilicate glass pipettes with filament (Harvard Apparatus; GC150F-10; o.d., 1.5 mm; i.d., 0.86 mm; 10-cm length). Recordings were made using MultiClamp700B amplifier (Molecular Devices), signals were filtered at 10 kHz (Bessel filter) and digitized (50 kHz) with a Digidata1440A and pClamp10 (Molecular Devices). For subsequent post hoc visualization, cells were filled with biocytin (Sigma-Aldrich, 2%) during recording.

(1) ChR experiments: All recordings were performed in presence of 10 µM GABA-A receptor blocker Gabazine (SR 95531; 6-imino-3-(4-methoxyphenyl)-1(6H)-pyridazinebutanoic acid hydrobromide; Tocris

Bioscience) in order to isolate excitatory currents and avoid disynaptic feedback inhibitory responses. Cells were held at a membrane potential of -70 mV. ChR-mCherry negative granule cells were identified and blue light was delivered using the CoolLED pE excitation system. For light simulation, single 2.5 ms long, 470 nm pulses were used and repeated 20 times at 0.2 Hz. Stimulus intensity was set to evoke maximal EPSC amplitudes. Recordings were analyzed using Clampfit 10.7. Events were included in analysis as synaptic if the maximal current amplitude was >5 pA within 20 ms following light stimulation.

(2) Perforant path stimulation: Patch-clamp recordings were made from CA3 pyramidal cells, while the perforant path was extracellularly stimulated with 1 ms long 5 mA current pulses at 0.2 Hz, for 3 min. For these recordings, 5 mM QX-314 was added to the intracellular solution and the extracellular ACSF contained 10 μM Gabazine. For each cell, evoked responses were averaged for quantification. Only one CA3 cell per slice was recorded.

In vivo electrophysiology

Male mice were used for in vivo electrophysiology, which were performed during light phase of the day cycle.

(1) Silicon probe implantation: For multichannel electrophysiological recordings, silicon probes (32- or 64-channel linear probes or polytrodes, Neuronexus, USA or Cambridge Neurotech, UK) were implanted 8-10 weeks after AAV-EGFP or AAV-Id2 injections. The surgery was performed under isoflurane anesthesia. After local disinfection (Betadine and 70% ethanol), the cranium was exposed and cleaned for application of adhesive agent (OptiBond XTR, Kerr Corporation, USA). Craniectomies were performed for stereotaxis-guided implantation of silicon probes into the dorsal hippocampus (-2.6 mm anterior/ posterior, and + 1.9 mm middle/lateral from bregma with tip in ventral/dorsal -2.2 to -2.45 mm from the brain surface). Probes were mounted on adjustable micro-drives. Before implantation, the probes were covered by DiI (Invitrogen, Life Technologies Corporation, USA) to allow histological verification. Implantations were performed using a micromanipulator (S-IVM-1000, Scientifica, UK). After implantation, craniectomies were sealed with artificial dura (Cambridge NeuroTech Ltd, UK). The probe-microdrive assemblies were covered with copper mesh to shield from electric noise in the environment. The mesh was covered by dental acrylate. Two stainless steel wires were inserted above the cerebellum as ground and reference for electrophysiological recordings. Recordings started after post-surgery recovery and habituation to connectorization.

(2) Data acquisition: Electrophysiological activity was registered using a multiplexing data acquisition system (Intan RHD2000-EVAL Amplifier Evaluation System, Intan Technologies, USA) at 20 kHz sampling rate. The position of the animal was tracked using a marker-based, high speed (120 frame/s) motion capture system and reconstructed in 3D (Motive, OptiTrack, NaturalPoint Inc, USA). Animals were recorded in open field for 20 min, preceded and followed by 30-90 min home cage recordings. After recordings, animals were transcardially perfused with 4% PFA in 0.1 M PB to confirm probe and AAV injection positions.

(3) Data analysis: Movement data were analyzed using MATLAB (MathWorks, USA). The speed of the animal was assessed from the euclidean distance between the coordinates in the horizontal plane, by calculating the harmonic mean in a sliding time window (0.083 s) and applying a Savitzky-Golay FIR smoothing filter. The speed data were further upsampled by linear interpolation from the 120 Hz sampling rate of the camera system to the sampling rate of local field potentials (LFP; 2 kHz). For LFP calculations, raw electrophysiological signals (sampling rate 20 kHz) were downsampled to 2 kHz after high-pass (cutoff frequency 0.5 Hz) zero-phase digital filtering. The signal from the pyramidal layer was selected based on the presence of ripples and histological verification of probe position.

(4) Calculation of LFP power: First, LFP signals recorded from the pyramidale, radiatum, lacunosum-moleculare, moleculare and hilus layers were decomposed using the Morlet-wavelet based algorithm (3) and their power spectrum was divided by the scale vector for bias rectification (4). Then, power spectrum was normalized by the sum of the total spectrum for each time point. The speed of the animal was binned into 0.25 cm/s bins, and the average of normalized power spectra at each speed bin was calculated. Then, data was grouped based on signal frequency into delta (1-5 Hz), theta (5-12 Hz), beta (15-35 Hz), slow

gamma (30-50 Hz), mid gamma (45-80 Hz), fast gamma (90-130 Hz), ripple (150-250 Hz), fast ripple (250-400 Hz) ranges, and speed-binned power spectra were summed within each frequency range. To acquire single power values, speed bins were divided into two speed ranges of locomotion (> 3 cm/s) and resting (< 3 cm/s), and the summed power spectra were averaged by the number of speed bins within each range.

(5) Detection of sharp wave-ripple (SWR) complexes: The magnitude of the Hilbert transform of the bandpass filtered (150-250 Hz) pyramidal layer signal (from which the mean of the signals from all recorded channels was subtracted beforehand) was used, after smooth averaging in 5 ms sliding windows. Ripple peaks were defined in the local maxima above 3 standard deviation (SD), event start and end points were considered when the signal increased above or decreased below 3 SD, respectively. Only events with a duration of >15 ms and <150 ms were used in further analysis. Time between two neighboring ripple peaks had to be at least 15 ms to be considered as separate; consecutive events with a time gap <15 ms were merged. Ripple amplitude was defined as the smoothed magnitude of the Hilbert transform in the time of ripple peaks, whereas ripple frequency was determined as the frequency with maximal power (estimated for each ripple event by Welch's method) above 100 Hz in the non-smoothed magnitude of the Hilbert transform between event start and end points. Only those ripples were analyzed which were detected in home cage recordings, when the speed of the animal was <3 cm/s and the signal of accelerometers incorporated in the recording head-stages did not change, i.e. during resting states. CSD around ripple peaks was calculated for all recorded hippocampal layers. Serving only visualization purposes, CSD maps were 100x upsampled by linear interpolation and smoothed by a Gaussian kernel. CSD maps and LPF averages around the ripple peaks were also used to confirm the anatomical layer from which signals were recorded; presence of sharp waves, and typical sinks and sources were indicative of radiatum, lacunosum-moleculare, moleculare and hilus. One representative channel was selected from all of these layers for further LFP power calculation.

(6) Dentate spike (DS) detection: Only home cage recordings were analyzed and when the speed of the animal was <3 cm/s and the signal of accelerometers did not change. LFP signals from the dentate molecular layer and hilus were de-trended (using a combination of polynomial curve fitting and polynomial evaluation, slow temporal fluctuations were removed from the signal), bandpass filtered (5-200 Hz) and z-scored. First, hilar signals were analyzed, and all events were detected which had local maximum > 3 standard deviation (SD) and a half width of 5-30 ms. The gap between consecutive local maxima had to be >20 ms to consider events as separate. Second, molecular layer signals were analyzed, and all events were detected which had local minimum >1 SD. An event was considered as DS when the time difference between the closest hilar positive and molecular negative peaks was <5 ms. Events <25 ms before or after SWRs were omitted. Then, DS-triggered CSD profiles were calculated from all molecular layer and hilar recording channels. To identify and separately analyze type-1 (DS1) and type-2 (DS2) events (5), first only in control (AAV-EGFP) mice, five recording channels were chosen as representative of molecular layer (3 channels) and hilus (2 channels) signals. In these, all DS events were pooled and separated into two clusters using k-means clustering in the 5x5 dimensional space (clustering into >2 k-means clusters did not reduce the total variation). Spikes in the cluster with lower mean CSD in the 2 molecular layer channels closest to hilus were considered as DS1, whereas spikes in the other cluster were considered as DS2. Visual inspection confirmed their identity as similar to those previously reported (5). DS events detected in AAV-Id2 injected animals were classified based on their shortest Euclidean distance from the centroids of DS1 and DS2 clusters recorded from control animals. In AAV-EGFP injected animals, 75% and 25% of all DS events were classified as DS1 and DS2, respectively, whereas in AAV-Id2, 92% and 8% of all DS events were classified DS1 and DS2, respectively.

Behavior

Male mice were used for behavioral tests. The animals were housed under a 12-12 h light-dark cycle, with lights on between 8:00 and 20:00. Before the tests, the animals were transferred to another facility and subjected to the inversion of their light cycle (12-12 hours of light-dark cycle with lights on between 20:00 and 08:00 next day). Tests were performed during the dark phase of the day cycle with indirect light of ~25 lux (except Barnes maze and fear conditioning, where it was 850 and 170 lux, respectively). Prior to tests, mice were handled ~3 min per day for 3 days. The movement of mice was video-recorded using

Ethovision and analyzed by a researcher blind to the injection scheme using AnyMaze, Wintrack (http://www.dpwolfer.ch/wintrack/) and R software.

(1) Home cage activity monitoring: To asses the adaptation to the new cycle the animals were recorded for 13 days under the new light cycle (light on at 20:00) using a rack of type II long mouse cages (365 mm long × 207 mm wide × 140 mm high) equipped with one passive IR sensor per mouse (ActiviScope, New Behavior Inc.). Home cage steady state data were collected during days 9, 10, 11, 12, and 13, which were the last 5 days of the total 13 days of observation.

(2) Open field test: A large white plastic box (48 cm × 48 cm × 33 cm; open on the top) was used as an open field area. The area of the open field was divided into an inner zone (30 × 30 cm) and a surrounding outer zone. Mice were place individually into the center of the open field and were allowed to freely explore for 20 min. The centre of the mouse body was used to track their movement. Between individuals, the maze was cleaned with deionized water. The following parameters (all based on AnyMaze readout) were scored: (i) to assess general locomotor activity: travel distance per 2 min segments and total distance, (ii) to evaluate the anxiety-like behavior: time spend in inner and outer zones, and travel distance in inner and outer zones.

(3) Novel object recognition test: This assay is designed to test object-related memory performance. One hour later after open field test, animals were allow to explore the open field arena again for 20 min. Training (acquisition) phase: 24 hours later, each mouse was placed again in the same environment, which now contained two identical objects (wooden balls), and allowed to freely explore for 10 min. Spatial cues were added on three walls of the open field box. Test (recognition) phase: 24 hours after training, each mouse was place again in the same environment, but now one object was replaced in the same location with a novel object (closed wooden tunnel). The test phase lasted for 10 min. Discrimination between the objects was calculated using a discrimination index (DI): DI = (time spent exploring the novel object - time spent exploring the familiar object) / the total time spent exploring the objects × 100. A mouse was considered to explore an object when its nose was actively touching the object but also when it was not more than 2 cm away from the object. Climbing on top of the object was not considered as exploration. As pre-established exclusion criteria, a mouse was not further considered for this analysis if DI>25% during test, reflecting bias.

(4) T-maze: This assay is designed to evaluate spontaneous alternation, short-term memory, and decision making. The T-maze had one ‚start' arm and the two ‚goal' arms (left and right; the dimensions of each arm were: length=28 cm, width=10 cm, wall hight=20 cm). The start arm also had a removable gate, whose removal was used to time the beginning of a trial. During each trial, the floor of the maze was covered with wood chipping litter. Each mouse was subject to three trials per day on two consecutive days. In one day, the three trials were separated by a one hour interval.

Each trial consisted of two consecutive phases: ‚sample' and ‚choice'. Sample phase: at the beginning of each trail, a flat wall barrier extending 18 cm into the start arm was lowered between the two goal arms, such that the mouse could enter either arm freely. The mouse was first placed in the start arm facing toward the goal arms and the gate was removed allowing the mouse freely enter either of the goal arms. Once the animal had entered one of the goal arms, the gate was slowly lowered such that the mouse could not exit the chosen arm and was allowed to freely explore the chosen arm for 30 sec. Choice phase: before this phase, the flat wall barrier between the two goal arms was removed. To begin this phase, the mouse was transferred back to start arm, again facing the goal arms, and the gate was removed allowing the mouse to freely enter either goal arms. A mouse was considered to enter an arm, when its whole body was inside that arm. The choice of the goal arm (left or right) as well as the time (latency) it took the mouse to enter that arm was recorded. A trial was discarded if latency to leave the start arm during sample or choice exceeded 2 min (1 trial).

A trial was counted as ‚successful' if the mouse entered different goal arms (alternation) during sample and choice, and ‚failed' otherwise. For each mouse, alternation rate was defined as the proportion of successful trials out of the total of six trials. Two mice (1 AAV-EGFP and 1 AAV-Id2) were excluded from final analysis, because they both skipped one choice and therefore their data series were incomplete.

(5) Morris water maze: This assay was designed to evaluate spatial memory performance. As pool, a circular white polypropylene enclosure (diameter=150 cm, wall height=68 cm) was used. As goal platform, a white quadratic object (14 cm × 14 cm × 14 cm) was placed in the middle of one quadrant, 30 cm from the side wall. The pool was filled with water (temperature=24–26°C, depth=15 cm) and mixed with milk until the platform was submerged (the surface of platform was 1 cm below water level) and became invisible. Spatial (visual) clues were placed on walls of the room. Each mouse underwent 6 training trials (with a max. duration of 2 min each trial) per day with intervals of 30–60 min for 5 consecutive days using a predefined sequence of different starting locations.

Days 1-3 (acquisition phase): the platform was placed always in the same position.

Days 4-5 (reversal phase): the platform was moved to the opposite quadrant. The first minute of the first reversal trial on day 4 served as the ‚1st probe trial' of reversal learning, to test for spatial retention; the first minute of the second trial on day 4 served as the ‚2nd probe trial' of reversal learning, that is to evaluate learning of the platform's new location. For each trial, the latency to reach the platform was measured by a tracking system. Mice that did not reach the platform within 2 min were removed from the pool by the experimenter.

(6) Barnes maze: This assay was designed to evaluate short- and long-term spatial memory performance. The Barnes maze was an elevated (65 cm above the floor of the room), blue, metal, circular platform with a diameter of 1 m. The platform contained 19 equally distanced holes (diameter=5 cm) around the perimeter. One of the holes had a hidden, black escape chamber underneath. Visual (spatial) cues were placed on walls of the room. During trials, bright lights (ca. 850 lux) were placed around the maze, prompting mice to look for a hiding place (escape chamber). As one-time habituation (2 min), each mouse was placed under a transparent box with access to only one (randomly chosen) hole with the escape chamber in order to habituate entering into the hole/chamber. Upon entering the escape chamber (i.e. all four paws were inside the chamber), they mice were placed back to their home cage, which represented a safe environment. 3 days after habituation, mice were trained to find and retreat in the escape chamber (3 trials per day, with a max. duration of 3 min each, with intervals of 60 min) for 5 consecutive days. Each trial started with placing the mouse under an opaque starting box in the centre of the platform. After 20 sec, the box was removed, and the animals were allowed to explore the maze and find the escape chamber.

For each trial, the amount of errors (primary and total), the escape-latency (primary and total) and search strategy were measured using an automated video tracking system. Primary errors were defined as head-deflections or pokes into incorrect holes before the first encounter (head-deflection or poke, but not necessarily enter had the mouse explored further) with the escape chamber. Total amount of errors was the number of errors made before the animal actually entered the escape chamber. Escape-latency was defined as the time required for the mice to make the first encounter with the escape chamber. Data from multiple same day trials were averaged per day.

Days 1-3 (acquisition phase; following habituation): each mouse performed 3 trials per day, during which the location of the escape chamber was randomly assigned for each mouse, and remained the same throughout all trials.

Day 4 (test phase): each mouse performed 4 trials. In the first trial (also referred to as probe trial), the escape chamber was removed, but the location was still considered as ‚correct target' for data acquisition. During trials 2-4, the escape chamber was placed under the hole on the opposite side of the escape position during acquisition, becoming the new ‚correct target' location for data acquisition. Thus, the first trial tested the spatial memory retention and confidence of mouse based on their experience on days 1-3, whereas trials 2-4 were used to evaluate their cognitive flexibility and short-term memory.

Day 5 (test phase): each mouse performed 3 trials. During trials 1-2, the escape chamber was placed in the same location for each mouse as on day 4. During trial 3 (probe trial), which was the last trial of the whole test, the escape chamber was again removed. Thus, trials 1-2 were used to evaluate the memory performance of the mouse based on their experience on day 4, whereas the last trial was used to evaluate the confidence of mouse regarding their spatial memory retention based on experience on days 4-5.

(7) Eight-arm radial maze: This assay was design to evaluate spatial reference and working memory performance. The eight-arm maze had a circular center platform (diameter=20 cm), which interconnected

eight, equally spaced arms (for each, length=36 cm, width=6.5 cm). Each arm had a cylindrical food cup at the end, presence or absence of food rewards was not visible from the center platform. The maze was elevated 37 cm above the floor of the room. All outside edges of the maze were walled by transparent plastic barriers (open on top) to prevent mice to look below the maze or to cross arms without fully entering the center platform, while allowing complete visibility of spatial cues. Spatial (visual) clues were placed on walls of the room. Throughout the assay, animals subject to a controlled feeding regime, so that they seek food pellets during trials. Mice were weighted daily and the amount of food was calculated to keep them on 85% of their body weight prior to the test. During each trial, 1 pellet of food reward (bait) was placed in each of the eight arms (i.e. total of 8 baits per trial). Mice were fed 30 min after trials.

Days 1-3 (food deprivation phase): to begin, mice were weighed for their initial bodyweight (BW). Then, each morning, mice were weighted to estimate the daily amount of food needed based on the initial bow (0.5 g food for 95-100% BW, 1 g for 95-90% BW, 2 g for 85-90% and 3g for < 85% BW).

Day 4 (habituation phase): each mouse was placed in the maze, and allowed to freely explore until five food pellets in five different arms were consumed, which was a threshold for task acquisition.

Days 5-14 (test phase): each mouse was placed in the maze, and allowed for 10 min to freely explore and consume food pellets. Mice were immediately removed from the maze when they consumed all eight of the available pellets. The strategy to find pellets (correct/incorrect arm entries as well as the order of arm entries) and time to consume all pellets were evaluated.

(8) Fear conditioning: The conditioning chamber (18cm x 18cm, Ugo Basile) was placed inside a sound attenuating enclosure, where a ventilation fan provided a background noise at ~55 dB. Each mouse was tested in three consecutive days. The movement/freezing of mice were recorded and analyzed with Ethovision (Noludus) and Wintrack in a two-step process. Step 1: Mouse activity was analyzed by EthoVision using frame-to-frame, pixel-by-pixel comparisons of the recorded video (25 Hz). A threshold parameter value of 17 was used, meaning that pixels of consecutive video frames were considered to be changed if their grey scale value differed by more than 17 on a scale of 255. In this manner, a new single image was created from every two consecutive video frame, containing the pixel level changes. In these images, the percentage of pixels that changed according to the above criteria was considered as the activity level of mouse corresponding to the time of images. Step 2: Using the EthoVision outputted images, freezing was scored by Wintrack as follow: (i) to reduce noise, pixel values in each image were normalized so that the smallest value equaled 0; (ii) freezing was scored in packages of 6 images (240 ms) and a package was considered as freezing if it fulfilled the following criteria: (a) the average image activity was ≤1%, (b) between two consecutive images the change was ≤0.07%, and (c) the highest and lowest activities in the package did not differ by >0.35% (these criteria ensured that activity level of the mouse was low and stable over time). Behaviorally-relevant freezing was considered and quantified as such if freezing episodes lasted at least 720 ms (3 packages, or 18 images) and subsequent freezing episodes were separated by activity bouts of at least 0.35% of cumulative activity. Statistical analyses were done in R.

Day 1 (training): each mouse was allowed to explore the chamber for 1 min and after which 3 tone-foot shock pairings (separated by 1 min intervals) were delivered. The tone (92 dB 2 kHz) lasted for 30 sec and the foot shock lasted for 2 sec (intensity: 0.5 mA; onset time: 28-30 sec of tone).

Day 2 (test): each mouse was tested for context (in the morning) and for cue (in the afternoon). For context, each mouse was placed back into the original conditioning chamber for 2 min. For cue, each mouse was placed into the same chamber with the following modifications, representing an altered context: the metal grid floor was replaced with a plastic plate floor, the plastic walls were covered with checkered pattern and a background odor was given by a stone wet of 1% lemon. Mice were allowed to freely explore the environment for 1 min, after which tone sounded for 1 min.

Day 3 (extinction): Each mouse was placed in the altered context chamber (same as in day 2 afternoon) and allowed to freely explore for 70 sec, after which 25 tones were delivered (each tone lasted for 30 sec, separated by 5 sec silent intervals).

Rat experiments

Wistar rats (Charles River Laboratories, 5 males and 3 females) were housed in groups. The temperature and relative humidity of the animal facility was kept at 22 ± 2°C and 60 ± 10%, respectively, and the

illumination followed the normal 12 h light/dark cycle with lights on at 8:00 A.M. The experiments were performed in accordance with the European Communities Council Directive of 2010 (2010/63/EU) and were reviewed and approved by the Hungarian NEBIH office (PE/EA/48-2/2020) and the Virus Safety Committee of the Institute of Experimental Medicine (20201029_2020119-20211119-0004).

Two-months old rats underwent stereotaxic surgery and bilateral viral construct injections into the ventral dentate gyrus (anterior-posterior -6.2 mm, medio/lateral ±4.7 mm, dorso/ventral -5.0 mm to bregma). All surgeries were performed under deep ketamine (50 mg/kg; Medicus Partner), xylazine (20 mg/kg; Medicus Partner), and pipolphen (0.2 ml/kg; Egis) anesthesia. The viral vectors (3:1 mixture of vWL74.AAVDJ8/2-mCaMKIIa-mId2-WPRE, 2.6×10^{13} vg/ml and rAAV8/hsyn-EGFP, 3.9×10^{12} vg/ml, UNC GTC Vectore Core; 500-500 nl volume/hemisphere, with 100 nl/min) were microinjected through a glass pipette by using a MicroSyringe Pump Controller System (World Precision Instruments). After the surgeries, rats received buprenorphine injection (Bupaq; 0.01 mg/kg) subcutaneously as analgesic treatment. Histological staining experiments were conducted 2-3 months after virus injection.

Rat brains were resectioned coronally into 60 μm thick sections. Timm staining was performed in every forth sections. ZnT3 staining was performed in the neighboring sections. Primary antibodies: Zinc transporter-3, guinea pig, polyclonal, Synaptic System, 197-004 (1:500); SLC30A3, rabbit Zinc transporter-3, polyclonal, ThermoFisher, PA-77769 (1:600). Secondary antibodies: Alexa Fluor 594 goat anti-guinea pig IgG (H+L) ThermoFisher, A11076 (1:500), Alexa Fluor 594 donkey anti-rabbit IgG (H+L) ThermoFisher, A21207 (1:500).

Statistical analysis

Statistical analyses were done using Python and Prism 9. All values represent mean ± standard error of the mean (SEM). The significance of differences was assessed using Welch's *t*-test, Mann-Whitney *U* test or one-way ANOVA, two-way ANOVA appropriately. Data distribution normality was tested by Shapiro-Wilk Test. Kolmogorov-Smirnov test was used to compare the cumulative distributions of two data sets. For normal distributions, Welch's *t*-test were performed. For non-normal distributions, non-parametric Mann-Whitney *U* test were performed. Significant main effects or interactions were followed up with post-hoc testing using original FDR method of Benjamini and Hochberg when applicable. The threshold for significance was p=0.05 or FDR=0.05, with a precise p value stated in each case; all tests were two-sided. Data analyses and quantifications were done blindly with respect to treatment.

Data availability

Sequencing data have been deposited to NCBI GEO under GSE161619.

References

1. C. Földy et al., Single-cell RNAseq reveals cell adhesion molecule profiles in electrophysiologically defined neurons. *Proc. Natl Acad. Sci. USA* **113**, E5222-31 (2016).
2. J. Winterer et al., Single-cell RNA-Seq characterization of anatomically identified OLM interneurons in different transgenic mouse lines. *European Journal of Neuroscience* **50**, 3750–3771 (2019).
3. C. Torrence, G. P. Compo, A practical guide to wavelet analysis. *Bull. Am. Meteorol. Soc.* **79**, 61–78 (1998).
4. Y. Liu, X. San Liang, R. H. Weisberg, Rectification of the bias in the wavelet power spectrum. *J. Atmos. Oceanic. Technol.* **24**, 2093–2102 (2007).
5. A. Bragin, G. Jandó, Z. Nádasdy, M. van Landeghem, G. Buzsáki, Dentate EEG spikes and associated interneuronal population bursts in the hippocampal hilar region of the rat. *J. Neurophysiol.* **73**, 1691-705 (1995).